



Recapitulating Evolutionary Divergence in a Single *Cis*-Regulatory Element Is Sufficient to Cause Expression Changes of the Lens Gene *Tdrd7*

Juliana G. Roscito ^{1,2,3} Kaushikaram Subramanian,^{1,3} Ronald Naumann,¹ Mihail Sarov,¹ Anna Shevchenko,¹ Aliona Bogdanova,¹ Thomas Kurth,⁴ Leo Foerster,^{1,2,3} Moritz Kreysing,^{1,3,5} and Michael Hiller ^{*,1,2,3}

¹Max Planck Institute of Molecular Cell Biology and Genetics, Dresden, Germany

²Max Planck Institute for the Physics of Complex Systems, Dresden, Germany

³Center for Systems Biology, Dresden, Germany

⁴Center for Molecular and Cellular Bioengineering, Technology Platform, TU, Dresden, Germany

⁵Center of Excellence, Physics of Life, Technical University, Dresden, Germany

*Corresponding author: E-mail: hiller@mpi-cbg.de.

Associate editor: Juliana G. Roscito

Abstract

Mutations in *cis*-regulatory elements play important roles for phenotypic changes during evolution. Eye degeneration in the blind mole rat (BMR; *Nannospalax galili*) and other subterranean mammals is significantly associated with widespread divergence of eye regulatory elements, but the effect of these regulatory mutations on eye development and function has not been explored. Here, we investigate the effect of mutations observed in the BMR sequence of a conserved noncoding element upstream of *Tdrd7*, a pleiotropic gene required for lens development and spermatogenesis. We first show that this conserved element is a transcriptional repressor in lens cells and that the BMR sequence partially lost repressor activity. Next, we recapitulated evolutionary changes in this element by precisely replacing the endogenous regulatory element in a mouse line by the orthologous BMR sequence with CRISPR–Cas9. Strikingly, this repressor replacement caused a more than 2-fold upregulation of *Tdrd7* in the developing lens; however, increased mRNA level does not result in a corresponding increase in TDRD7 protein nor an obvious lens phenotype, possibly explained by buffering at the posttranscriptional level. Our results are consistent with eye degeneration in subterranean mammals having a polygenic basis where many small-effect mutations in different eye-regulatory elements collectively contribute to phenotypic differences.

Key words: *cis*-regulatory elements, phenotypic evolution, genome engineering, eye degeneration, subterranean mammals.

Introduction

Colonization of new habitats, such as the underground environment, is often linked to morphological, physiological, and behavioral adaptations that confer advantages in the new habitat. Among mammals, the naked mole rat, blind mole rat (BMR), star-nosed mole, and cape golden mole comprise four distinct lineages that have independently evolved adaptations to live in such constantly dark (or poorly illuminated) environments. One of the most striking adaptations of these subterranean mammals is the reduction or loss of the visual system, evident by the presence of a degenerated lens and retina, as well as a reduction of the visual-processing area of the brain (Sweet 1909; Sanyal et al. 1990; Cooper et al. 1993a, 1993b; Catania 1999; Hetling et al. 2005; Nevo 2007; Némec et al. 2008).

Genetically, the degeneration of the visual system is related to mutations in eye-related genes. Previous studies that investigated the genomes of subterranean mammals showed that many genes involved in eye development and function are diverged or lost in these species (Kim et al. 2011; Emerling and Springer 2014; Fang, Nevo, et al. 2014; Fang, Seim, et al. 2014; Prudent et al. 2016; Sharma and Hiller 2020). Naturally occurring or laboratory-induced gene-inactivating mutations in some of these genes in humans or mice cause malformation of eye structures and impaired vision (Hansen et al. 2007; Abd El-Aziz et al. 2008; Makiyama et al. 2014; Emerling et al. 2017; Moore et al. 2018), suggesting that the gene losses observed in subterranean mammals contributed to the evolution of degenerated eyes.

© The Author(s) 2020. Published by Oxford University Press on behalf of the Society for Molecular Biology and Evolution.

This is an Open Access article distributed under the terms of the Creative Commons Attribution Non-Commercial License (<http://creativecommons.org/licenses/by-nc/4.0/>), which permits non-commercial re-use, distribution, and reproduction in any medium, provided the original work is properly cited. For commercial re-use, please contact journals.permissions@oup.com

Open Access

In addition to the widespread loss of genes, recent studies discovered divergence in many eye regulatory elements (Partha et al. 2017; Langer et al. 2018; Roscito et al. 2018; Langer and Hiller 2019). In particular, genome-wide analysis of conserved noncoding elements (CNEs) revealed that CNEs with preferential sequence divergence in subterranean mammals are significantly associated with eye-related genes and significantly overlap regulatory elements that are active in developing and adult eyes of mice or humans (Roscito et al. 2018). Sequence divergence in these CNEs also resulted in a large-scale divergence of binding sites of eye-related transcription factors (TFs) (Langer et al. 2018; Roscito et al. 2018; Langer and Hiller 2019). Together, this suggests that widespread divergence in both genes and in *cis*-regulatory elements may have contributed to the degeneration of eye structures in subterranean mammals, leading to a greatly impaired visual system.

In protein-coding genes, premature stop codon, frameshift, or other reading frame-inactivating mutations can be considered as equivalent if they result in a nonfunctional protein. This makes it possible to use phenotypes observed in mouse knockout lines or human individuals with inactivated genes to infer the effect of evolutionary gene losses, even though the identity of the underlying inactivating mutations is different. In contrast to genes, where inactivating mutations are often predictable, the effects of mutations in *cis*-regulatory elements are less clear and mostly unexplored. In particular, it is hard to predict how, and to what extent, mutations in regulatory elements affect its activity and how such activity changes in turn affect the expression of its target gene. Consequently, to understand the effect of mutations in a regulatory element *in vivo*, it is necessary to precisely recapitulate the naturally occurring mutations on a model organism and quantify the consequences at the molecular and morphological level. Considering the importance of *cis*-regulatory changes for morphological evolution (Wray 2007; Carroll 2008), characterizing the effect of naturally occurring mutations in regulatory elements *in vivo* is crucial to understand the evolution of phenotypic traits.

To explore the effect of regulatory divergence on eye degeneration in subterranean mammals, we focused on a lens regulatory element near *Tdrd7* (tudor domain-containing 7), a gene essential for lens development and spermatogenesis. We used CRISPR–Cas9 to precisely replace the mouse sequence of this regulatory element by the BMR sequence and characterized the molecular and morphological effects of the mutations observed in the BMR on lens development and function.

Results

Divergence in a Lens Regulatory Element Near *Tdrd7*

In previous studies, we used two comparative genomics approaches to identify and associate sequence and TF-binding site divergence in CNEs to the vision-impaired phenotype of the subterranean BMR, naked mole rat, cape golden mole, and star-nosed mole (Langer et al. 2018; Roscito et al. 2018). Both screens detected significantly higher

sequence and binding site divergence in subterranean mammals in a locus that comprises two CNEs located 97 bp from each other (fig. 1A and B). These CNEs are part of a larger 339 bp region that evolves under constraint according to GERP++ (Davydov et al. 2010). Higher sequence divergence is evident in the star-nosed mole, cape golden mole and, most prominently, in the BMR (*Nannospalax galili*), which exhibits a 197 bp deletion (fig. 1A and B).

In mouse, this larger CNE overlaps many epigenetic marks derived from embryonic and adult mouse eye tissues (fig. 1C). In particular, we observe ChIP-seq peaks for eye TFs such as OTX2, CRX, and NRL (Corbo et al. 2010; Hao et al. 2012; Samuel et al. 2014). In addition, the mouse sequence has predicted binding sites for TFs relevant for eye development, such as PITX2, CMAF, HSF1, and PAX2, three of those sites overlapping the large BMR deletion (fig. 1D). Furthermore, this region overlaps ATAC-seq and DNaseI hypersensitivity peaks in adult eye tissues (Encode Project Consortium 2012; Mo et al. 2016; Zhao et al. 2019) as well as a prominent lens-specific ATAC-seq peak in developing mouse lens (Roscito et al. 2018) (fig. 1C). Together, this indicates that the CNE may function as a regulatory element in lens tissue.

This CNE is located ~4.5 kb upstream of the conserved transcription start site of *Tdrd7* (fig. 1C), a gene that is highly expressed in lens and testis (Hosokawa et al. 2007; Lachke et al. 2011; Tanaka et al. 2011). The encoded TDRD7 protein is a component of cytoplasmic ribonucleoprotein granules that are involved in the posttranscriptional control of genes critical for lens development and spermatogenesis (Lachke et al. 2011; Tanaka et al. 2011). Mouse studies showed that knock-down or loss-of-function mutations in *Tdrd7* lead to lens malformation, cataracts, and glaucoma (Lachke et al. 2011). In addition, male *Tdrd7* knockout mice are sterile due to an arrest in spermatogenesis (Tanaka et al. 2011). Human individuals carrying TDRD7 loss-of-function mutations also exhibit cataracts and azoospermia (Lachke et al. 2011; Tan et al. 2019). Thus, *Tdrd7* is essential for normal lens development and function and spermatogenesis. Importantly, in contrast to divergence of the CNE sequence, *Tdrd7* is intact in all subterranean mammals, including the BMR, likely because of its pleiotropic role in lens development and fertility.

The close proximity to a gene required for normal lens development, and the overlap with several epigenetic marks identified in different eye tissues suggest that the genomic locus containing the diverged CNE may function as a regulatory element controlling *Tdrd7* expression. Our observation that this CNE is highly diverged in a subterranean mammal with degenerated lenses makes this CNE a promising candidate to test whether the naturally occurring mutations have an effect on *Tdrd7* expression and normal development or function of the lens. Furthermore, there is no other CNE that is diverged in subterranean mammals and overlaps epigenomic marks from eye tissues in a 500 kb window around the *Tdrd7* promoter.

The *Tdrd7* CNE Acts as a Transcriptional Repressor in Mouse Lens Cells

We first tested the mouse and BMR sequences for regulatory activity, using an *in vitro* dual luciferase reporter gene assay in

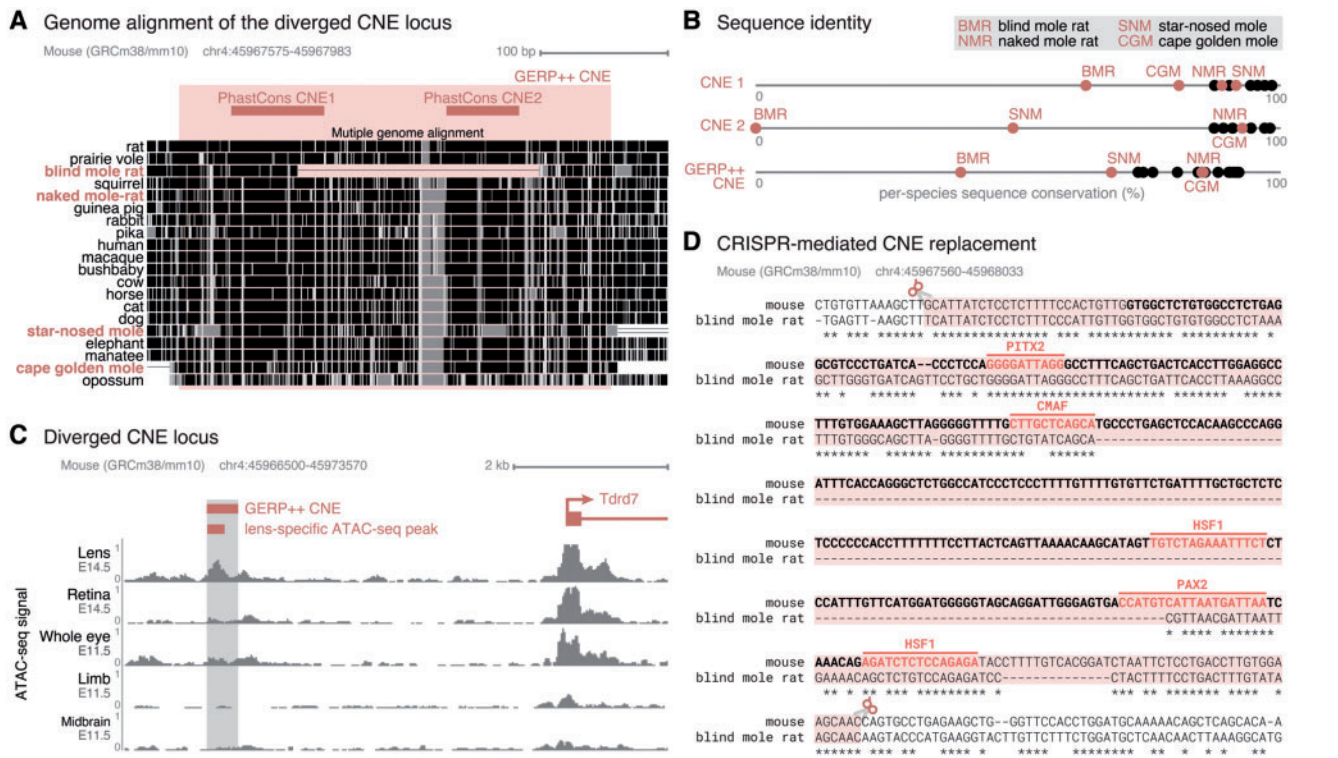


FIG. 1. Divergence in a lens regulatory element near *Tdrd7* in subterranean mammals. (A) Multiple genome alignment, showing the two diverged CNEs detected with PhastCons and the larger CNE detected with GERP++ that encompasses both PhastCons CNEs. In the multiple genome alignment, aligning sequence is visualized by black and gray boxes. The darker the color of the box, the higher is the sequence similarity in the alignment. The subterranean vision-impaired species are highlighted in red. (B) Sequence divergence plot of the conserved elements shown in (A). The x-axis shows the percent identity between the CNE sequence of a species and the reconstructed placental mammal ancestor. Subterranean mammals are represented by red dots, all other mammals by black dots. The star-nosed mole, cape golden mole and, most prominently, the BMR exhibit more diverged CNE(s) compared with other mammals. (C) Overview of the larger genomic context, showing the GERP++ CNE, the *Tdrd7* gene located ~4.5 kb downstream and ATAC-seq signal tracks of different developing mouse tissues. The CNE overlaps an ATAC-seq peak observed in lens of E14.5 mice. (D) Alignment between mouse and BMR sequence encompassing the GERP++ CNE. The mouse CNE sequence is in bold. The sequence highlighted by the red box corresponds to the genomic mouse sequence that was replaced by the orthologous BMR sequence with CRISPR–Cas9. Predicted TF-binding motifs are highlighted in the mouse sequence.

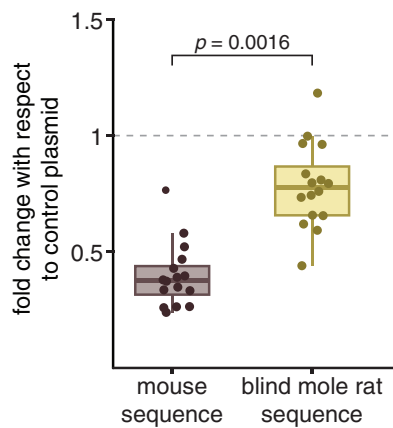


FIG. 2. Partial loss of repressor activity of the BMR CNE sequence. In vitro dual luciferase assay shows that the BMR sequence (yellow) of the *Tdrd7* CNE exhibits a significantly weaker repressor activity than the mouse sequence (purple). Expression values correspond to the fold change with respect to the control plasmid that lacks any sequence insert upstream of the promoter. The *P* value was computed with a two-sided Wilcoxon rank sum test.

a lens cell line. We cloned both sequences in the same genomic orientation with respect to the *Tdrd7* promoter into a firefly luciferase vector, cotransfected this vector with a control renilla luciferase vector into lens cells, and measured firefly luciferase expression driven by the mouse and BMR sequences. This experiment revealed that the mouse sequence is indeed a regulatory element (fig 2). Interestingly, the mouse sequence acts as a repressor element, as firefly luciferase expression was significantly below the expression obtained with a control vector that does not contain any sequence insert upstream of the promoter. The expression driven by the BMR sequence was also lower than the control vector expression, but was significantly higher than the mouse sequence. This observation suggests that sequence changes, including the larger deletion observed in the BMR sequence, result in a partial release of repressor activity.

Recapitulating Evolutionary Changes in This Lens Regulatory Element in Mouse

The observed partial loss of repressor activity of the BMR sequence predicts that replacing the mouse genomic sequence of this regulatory element by the BMR sequence

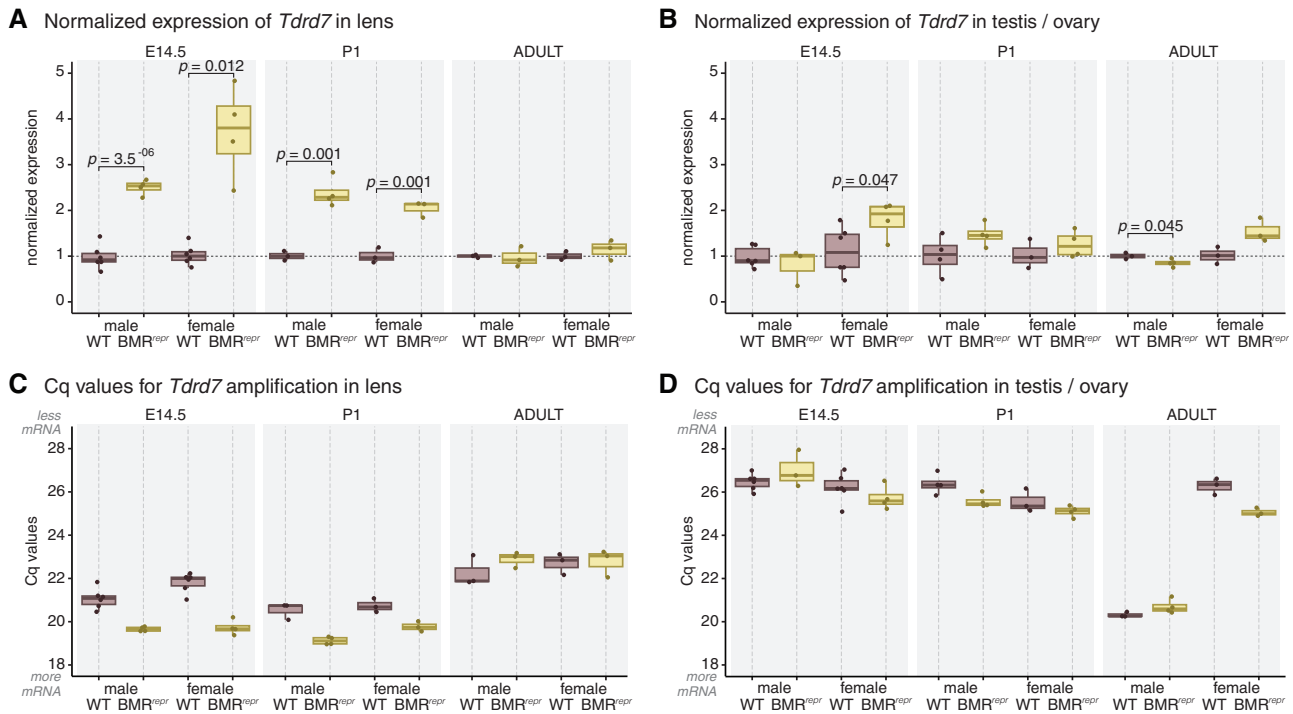


FIG. 3. *Tdrd7* is upregulated in developing lens of *BMR^{repr}* mice. (A, B) Comparison of *Tdrd7* expression in developing and adult lens (A) and reproductive organs (B) of wild-type (purple) and *BMR^{repr}* mice (yellow) with RT-qPCR. The strongest difference is a more than 2-fold upregulation of *Tdrd7* in developing lens of *BMR^{repr}* mice. Expression values were normalized by the housekeeping gene *Rpl13a* and by the levels of wild-type mice. Each data point is a biological replicate. *P* values were computed with a two-sided *t*-test. (C, D) Comparison of Cq values indicate that *Tdrd7* mRNA is more abundant in the lens and adult testis than in the developing testis or ovary.

may result in an upregulation of *Tdrd7*. To test this in vivo, we created a transgenic mouse line (referred hereafter as *BMR^{repr}* mice) in which we recapitulated the naturally occurring BMR mutations in this repressor element. To this end, we used CRISPR–Cas9 to precisely replace the 410-bp endogenous mouse sequence encompassing the lens regulatory element with the orthologous BMR sequence (fig. 1D). Compared with the luciferase assay, this approach allows us to assess the effect of the BMR mutations in the full genomic context with the native *Tdrd7* promoter. We used C57BL/6j mice because the N strain already carries a mutation in the photoreceptor *Crb1* gene, resulting in retinal degeneration (Mattapallil et al. 2012). *BMR^{repr}* mice were born at normal Mendelian ratios, were viable and showed no obvious phenotype. In particular, *BMR^{repr}* mice showed no abnormality in sperm quality compared with wild-type mice (supplementary table 1, Supplementary Material online) and exhibited normal fertility (supplementary table 2, Supplementary Material online), suggesting that this repressor element does not affect spermatogenesis and reproduction. In the following, we used the *BMR^{repr}* mouse line to quantify the molecular and morphological effects of evolutionary divergence in this lens regulatory element.

Tdrd7 Is Upregulated in the Developing Lens of *BMR^{repr}* Mice

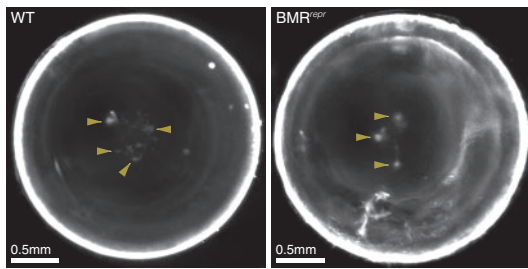
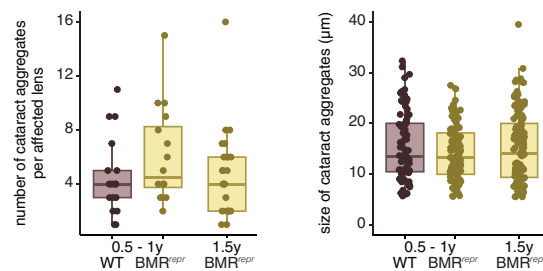
To validate the partial loss of lens repressor activity of the BMR sequence in vivo and to test whether the observed repressor activity difference affects *Tdrd7* expression in the

lens, we used RT-qPCR to compare the expression of *Tdrd7* in wild-type and homozygous *BMR^{repr}* mice at three different time points, embryonic day 14.5 (E14.5), postnatal day 1 (P1), and 3 months (adult). Since *Tdrd7* has an additional role in spermatogenesis, we also quantified its expression in the testis and ovaries at the same time points.

We found that *Tdrd7* is consistently and significantly upregulated in the lens of E14.5 and P1 *BMR^{repr}* mice in comparison with wild-type mice (fig. 3A). No differences in *Tdrd7* expression were observed in adult lens. We also observed a small but marginally significant downregulation of *Tdrd7* in adult but not developing testes, and a marginally significant upregulation in developing ovaries (fig. 3B). Despite *Tdrd7* expression changes in reproductive organs, increased *Tdrd7* expression is consistently observed in developing lenses of male and female mice, and the magnitude of *Tdrd7* upregulation is substantially higher in the lens compared with the magnitude of *Tdrd7* expression differences in testis and ovary (fig. 3A and B). Furthermore, the absolute expression level in ovaries of wild-type and *BMR^{repr}* mice is substantially lower than in the lens (fig. 3C and D). Together with the ATAC-seq data and luciferase reporter assays, this suggests that the major function of the regulatory element is to suppress *Tdrd7* expression in the developing lens.

BMR^{repr} Mice Have No Obvious Lens Phenotype

Knock-down and loss-of-function mutations in *Tdrd7* have been shown to impair normal lens morphology and function (Lachke et al. 2011; Tanaka et al. 2011), but the morphological

A Lenses under darkfield microscopy**B** Quantification of cataract aggregates**C** Scanning electron microscopy

Wild-type lens

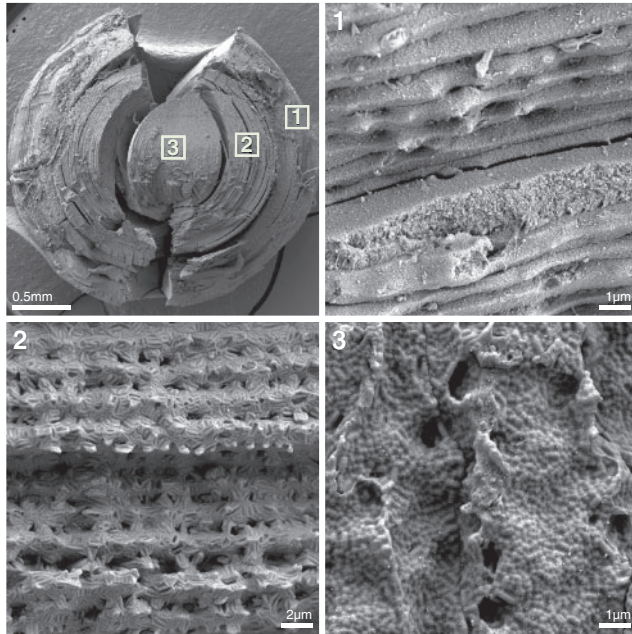
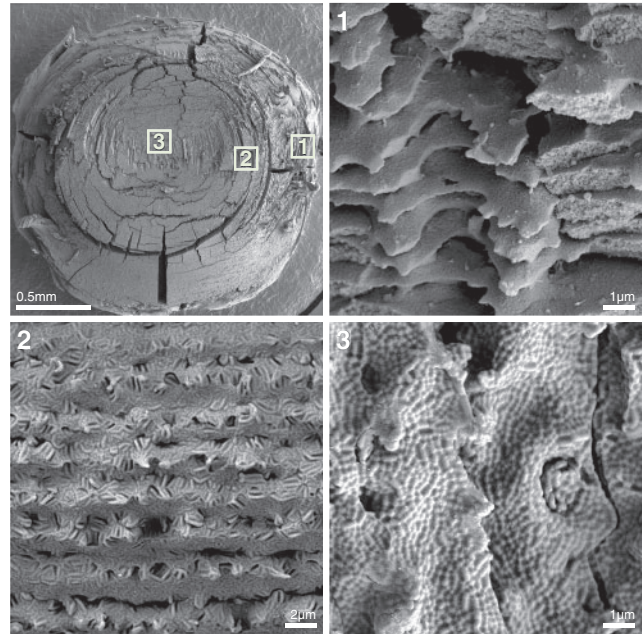
BMR^{repr} lens

Fig. 4. BMR^{repr} mice do not show an obvious lens phenotype. (A) Lenses of wild-type and BMR^{repr} mice viewed under darkfield illumination exemplify cataract aggregates (yellow arrowheads) in the center. (B) Quantification of the number and size of cataract aggregates in age-matched (0.5–1 year old) wild-type (purple) and BMR^{repr} (yellow) mice shows that BMR^{repr} mice have a slightly higher number of similarly sized cataract aggregates (differences are not statistically significant). We additionally analyzed 24 lenses of 1.5-year-old BMR^{repr} mice and these showed no increase in number or size of cataract aggregates compared with younger BMR^{repr} mice. (C) Comparison of lens fibers in 2-year-old wild-type and BMR^{repr} mice with scanning electron microscopy shows no obvious morphological differences. Different areas of the lens, highlighted by boxes with numbers 1–3 at the top left most image, are represented in closer detail in the remaining images.

effects of overexpression of *Tdrd7* have not yet been investigated. Therefore, we analyzed whether the observed increase in *Tdrd7* expression in the developing lens of homozygous BMR^{repr} mice affects lens function and morphology.

We first investigated whether lenses of adult BMR^{repr} mice exhibit signs of cataracts, a clouding of parts of the lens caused by aggregation of lens proteins (Remington 2012). To this end, we carefully dissected lenses of wild-type and BMR^{repr} mice, imaged them under darkfield illumination and quantified opaque cataract aggregates in the core of the lens, which is the only place where we observed such aggregates (fig. 4A). As shown in figure 4B, we found that BMR^{repr} mice have a slightly higher number of cataract aggregates compared with wild-type mice (average 6.06 vs. 4.47; Wilcoxon two-sided rank test *P* value of 0.18). The size of cataract aggregates is slightly lower in BMR^{repr} compared with wild-type mice

(average 14.2 μm vs. 15.5 μm; Wilcoxon two-sided rank test *P* value of 0.33). To test whether the subtle difference in cataract aggregate number is augmented in older BMR^{repr} mice, we analyzed individuals older than 1.5 years, but found no increase (fig. 4B).

Next, we investigated whether lens fibers of BMR^{repr} mice exhibit structural changes compared with those of wild-type mice. The lens is composed of multiple concentric layers of tightly connected fibers. The fiber membranes have numerous and complex interdigitations and cell–cell junctions, resulting in a rigidly structured epithelium that is important for lens function by minimizing the spacing between fibers and, thus, minimizing light scattering (Remington 2012). We used scanning electron microscopy to image the morphology of the lens fibers of adult mice and compared the outer, median, and inner layers of the lenses. As shown in

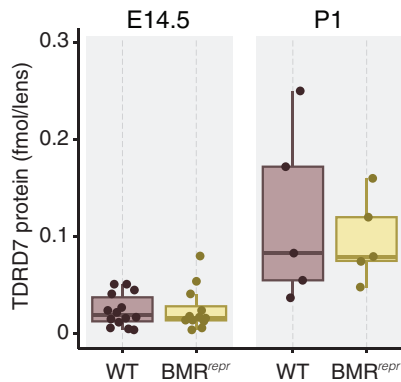


Fig. 5. *Tdrd7* expression differences in BMR^{repr} mice are buffered at the protein level. Absolute quantification of TDRD7 protein in the lenses of E14.5 and P1 wild-type (purple) and BMR^{repr} mice (yellow) shows a similar TDRD7 protein content.

figure 4C, there is no obvious difference in shape or fiber arrangement between wild-type and BMR^{repr} mice.

Together, these analyses show that the substantial increase in *Tdrd7* expression in the developing lens of BMR^{repr} does not result in a clearly detectable lens phenotype.

Upregulation of *Tdrd7* Does Not Result in an Increased TDRD7 Protein Content

Given the lack of an obvious lens-related phenotype, we investigated whether the significantly increased *Tdrd7* mRNA levels in the lens of BMR^{repr} mice lead to an increase in TDRD7 protein levels. To this end, we used mass spectrometry to precisely quantify the absolute amount of TDRD7 in the lens of wild-type and homozygous BMR^{repr} mice at E14.5 and P1, the two time points where *Tdrd7* mRNA expression is significantly increased. Surprisingly, we observed a similar amount of TDRD7 protein in the lens of wild-type and BMR^{repr} mice (fig. 5). This indicates that differences in *Tdrd7* expression are effectively buffered at the protein level by a currently unknown mechanism. The absence of significantly different protein levels provides an explanation of why the embryonic misregulation of *Tdrd7* in the lens of BMR^{repr} mice does not result in a detectable lens phenotype.

Discussion

Comparative genome analysis has revealed many associations between particular traits and genomic changes in particular genes or regulatory elements. Understanding the contribution of mutations in such genes or regulatory elements to the evolution of a trait requires an experimentally tractable system, such as the mouse, where specific mutations can be introduced and their effects quantified. Gene knockout studies in mice contributed to our understanding of the functional role of many genes naturally lost in a variety of mammalian species (Meredith et al. 2009; Gaudry et al. 2017; Meyer et al. 2018; Sharma, Hecker, et al. 2018; Sharma and Hiller 2018; Sharma, Lehmann, et al. 2018; Hecker et al. 2019; Huelsmann et al. 2019). However, the effect of other, much more frequent genomic changes, such as amino-acid changing mutations in protein-coding sequences and

sequence changes in regulatory elements has rarely been explored.

Here, we experimentally investigated the effects of prominent mutations in a lens regulatory element that were observed in the BMR, a burrowing mammal with greatly reduced eyes. To this end, we used CRISPR–Cas9 to precisely replace the mouse sequence of this regulatory element by the BMR sequence. Consistent with our *in vitro* results showing that the BMR sequence exhibits a partial loss of repressor activity in lens cells, we found that BMR^{repr} mice exhibit an upregulation of the *Tdrd7* gene in the developing lens. This indicates that a transcriptional repressor element plays a role in controlling *Tdrd7* expression in the developing lens in mice, which reveals an unknown aspect of *Tdrd7* regulation. As the repressor element exhibits sequence conservation in most other mammals, this repressing activity may be conserved in other mammals.

Strikingly, we found that replacing the sequence of this single regulatory element is sufficient to cause a more than 2-fold increase in expression, which reveals that this repressor element has a major effect on *Tdrd7* expression. This result contrasts previous findings that perturbations of individual regulatory elements generally have no measurable or only a small effect on gene expression (Ahituv et al. 2007; Cretekos et al. 2008; Capellini et al. 2017; Osterwalder et al. 2018; Sarro et al. 2018; Thompson et al. 2018; Fulco et al. 2019). Previously observed robustness at the transcriptional level can be attributed to functional redundancy, whereby multiple regulatory elements control the expression of a gene and a substantial change in gene expression can only be achieved by perturbations of multiple elements (Osterwalder et al. 2018). Importantly, whereas expression robustness of other genes may be achieved at the transcriptional level, our observations that the large increase in *Tdrd7* mRNA does not lead to a corresponding increase in protein raises the possibility that robustness of TDRD7 protein expression is instead achieved at the posttranscriptional level. Buffering mechanisms at the protein level are quite frequent, especially for proteins that are part of protein complexes (Stingele et al. 2012). Which mechanisms confer posttranscriptional buffering of increased *Tdrd7* mRNA levels are currently unknown and remain to be investigated.

The absence of increased TDRD7 protein levels in the lens likely explains why BMR^{repr} mice do not exhibit an obvious lens phenotype. Nevertheless, it is possible that these animals exhibit more subtle phenotypes for which it is hard to detect significant differences with a limited number of individuals. For example, we observed that BMR^{repr} mice exhibit slightly more cataract aggregates in the lens; however, many more individuals would be needed to assess whether this subtle difference is consistently observed (a power analysis indicates that one would need to analyze at least 63 lenses of wild-type and of BMR^{repr} mice to achieve statistically significant result). In addition, more pronounced phenotypes may not be expressed under the constant conditions of the artificial laboratory environment. In contrast, in the wild, where environmental fluctuations occur, pathogens exist, and food and mating partners are limited, both subtle as well as

condition-dependent phenotypes would be subjected to natural selection over longer periods of time.

Although perturbations or deletions of single regulatory elements can result in drastic (Chan et al. 2010; Kvon et al. 2016; Gonen et al. 2018) or subtle phenotypic changes (Cretekos et al. 2008; Capellini et al. 2017; Thompson et al. 2018), they most often do not result in a detectable phenotype (Ahituv et al. 2007; Frankel et al. 2010; Osterwalder et al. 2018; Sarro et al. 2018). However, mutations in several regulatory elements can collectively account for phenotypic differences. For example, most mutations associated with complex traits and diseases are located in noncoding, presumably regulatory, genomic regions (Zhang and Lupski 2015; Guo et al. 2017). Individually, most of these mutations have a small effect, but collectively they can explain a large portion of the heritability of complex traits (International Schizophrenia Consortium et al. 2009; Yang et al. 2010; Fuchsberger et al. 2016; Castro et al. 2019). Similarly, our study showed that perturbing a single lens repressor element in a model organism leads to a molecular phenotype (gene expression change), but does not result in a detectable organismal phenotype, likely because the entire genetic machinery required for functional eyes is intact in mice. However, we have previously shown that numerous components of the genetic “eye-making” machinery are highly diverged in the BMR and other subterranean mammals, as these species lost several eye-related genes and exhibit divergence in hundreds of eye regulatory elements (Langer et al. 2018; Roscito et al. 2018; Langer and Hiller 2019). This has several, not mutually exclusive implications. First, due to relaxation of constraint, mutations in the *Tdrd7* lens repressor may have occurred (or were only permitted) after eye degeneration had reached an advanced state in the BMR lineage. Under this possibility, these mutations were not primarily involved in eye phenotypes, but are a consequence of eye degeneration. A second possibility is that these mutations made a (potentially small) contribution to eye degeneration in the subterranean BMR lineage, but if this trait has a polygenic basis, one would need to recapitulate perturbations in several regulatory elements, in addition to the *Tdrd7* lens repressor, to recapitulate BMR eye phenotypes.

In the BMR *Tdrd7* gene locus, the CNE overlapping the lens repressor exhibits the strongest divergence signature. Nevertheless, additional mutations likely occurred (before or after the repressor element mutations) in this locus during BMR evolution, some of which may have also altered *Tdrd7* expression. As expression of a gene is determined by the collective input of its regulatory elements, we cannot infer which effect the regulatory mutations investigated here have on *Tdrd7* expression in the embryonic lens of extant BMRs, since this would require an understanding of how other regulatory mutations influence its expression level. Still, ongoing advances in genome engineering (Grunwald et al. 2019) will make it easier to test this in future by introducing additional regulatory mutations (in the *Tdrd7* as well as in other loci) in the BMR^{repp} mouse line. Such studies will expand our understanding of the effect of perturbations of individual regulatory elements and regulatory robustness, and could ultimately

enable predictions of which and how many perturbations are required to cause a particular phenotypic difference.

Materials and Methods

Computational Identification of *Tdrd7* Regulatory Locus

Two CNEs upstream of *Tdrd7* were identified in two previous genome-wide screens for CNEs that are diverged in subterranean mammals (Langer et al. 2018; Roscito et al. 2018). In the first screen, we generated a multiple whole-genome alignment with mouse (mm10 assembly) as the reference and 24 other mammals, used PhastCons (Siepel et al. 2005) to obtain conserved regions, and extracted CNEs by excluding protein-coding regions. This resulted in 351,279 CNEs. For each CNE, we then used the Forward Genomics branch method (Prudent et al. 2016) to assess whether the CNE sequence is preferentially diverged in subterranean mammals (Roscito et al. 2018). In the second screen, we considered the same set of CNEs, but determined whether a CNE exhibits preferential divergence of eye TF-binding sites using REforge (Langer et al. 2018). Applying GERP++ (Davydov et al. 2010), another method to determine evolutionary constraint, to the same multiple genome alignment shows that both PhastCons CNE are part of a larger GERP++ CNE. To determine whether this CNE overlaps previously published regulatory data, we mapped ChIP-seq, DNase-seq, and ATAC-seq data (Corbo et al. 2010; Encode Project Consortium 2012; Hao et al. 2012; Samuel et al. 2014; Mo et al. 2016; Roscito et al. 2018; Zhao et al. 2019) derived from developing and adult mouse eye tissues to the mouse mm10 assembly using the bedtools suite (Quinlan and Hall 2010). We inferred TF-binding sites using MAST (Bailey and Gribskov 1998) with a previously obtained set of 28 eye TFs (Langer et al. 2018).

In Vitro Test for Regulatory Activity with a Dual Luciferase Reporter Assay

We synthesized and cloned a 410-bp mouse sequence that spans both diverged CNEs (mm10 assembly; chr4:45967574–45967983) and the orthologous 208-bp BMR sequence (nanGal1 assembly; KL203377:255659–255866) into a luciferase pGL4.23[luc2/minP] vector (Promega, USA). We cloned the insert in the same orientation with respect to the minP promoter and luciferase gene as the CNE and the *Tdrd7* promoter are oriented in the genome. We used the renilla pGL4.73 [hRluc/SV40] (Promega, USA) as the control plasmid.

We obtained an aliquot of a primary culture of 21EM15 mouse lens cells for this experiment (kind gift from Dr Salil Lachke). These cells were cultured in DMEM (Thermo Fisher Scientific, USA) supplemented with 10% fetal bovine serum (Merck, Germany), at 37 °C, 5% CO₂, and 100% humidity. For detachment, cells were washed with phosphate-buffered saline (PBS) and treated with 0.05% Trypsin/EDTA (Thermo Fisher Scientific, USA) for 3 min at 37 °C. After incubation, fresh medium was added, spun down at 140 g for 5 min and resuspended in fresh complete media; 3,000 cells/well were seeded into the 384-well plate (Corning, USA). The enhancer

constructs were transfected 24 h after seeding using FuGENE6 (Promega, USA) as the transfection reagent, following manufacturer's instructions. In brief, FuGENE6 was mixed in OptiMEM (Thermo Fisher Scientific, USA) and incubated for 5 min at room temperature. The plasmids with firefly and renilla luciferases were added to the mix in a ratio of 100:1 and, after an incubation period of 20 min at room temperature, the transfection complex was added to the cells in a 4:1 FuGENE/DNA ratio. The luminescence read-out was obtained 48 h after transfection, using the Dual-Glo Luciferase Assay System Kit (Promega, USA) as substrate, according to manufacturer's instructions, and an Envision 2104 Multilabel reader (Perkin Elmer, USA) with an ultrasensitive luminescence 384-well aperture.

We repeated the assay twice (two different plates) with a total of eight technical replicates per plate for each of the mouse and BMR tested sequences. The ratio of firefly and renilla luciferases was normalized by the mean of the replicates of the empty control vector of the respective plate. Significance was assessed using a two-sided Wilcoxon rank sum test.

Mouse Transgenics

Ethics Statement

Work with mouse was performed in accordance with the German animal welfare legislation and in strict pathogen-free conditions in the animal facility of the Max Planck Institute of Molecular Cell Biology and Genetics, Dresden, Germany. Protocols were approved by the Institutional Animal Welfare Officer (Tierschutzbeauftragter), and necessary licenses were obtained from the regional Ethical Commission for Animal Experimentation (Landesdirektion Sachsen, Dresden, Germany).

CRISPR Guide Design. To measure the molecular and morphological effects of divergence in the *Tdr7* regulatory locus, we used the CRISPR–Cas9 system to create a transgenic mouse line in which we replaced the aforementioned 410-bp mouse sequence by the orthologous 208-bp BMR sequence. We designed four guide RNAs to target the *Tdr7* locus for the CRISPR transgenesis using the Geneious software (8.1.6; Biomatters), and created a repair construct comprising 500-bp homology arms flanking the 208-bp BMR sequence. Guide sequences (PAM sequence underlined) and repair construct sequence (BMR sequence underlined) are the following: gRNA1: 5'-GTTTCATGGATGGGGGTAGCAGG-3'; gRNA2: 5'-TGATTAATCATTAAATGACATGG-3'; gRNA3: 5'-TAATCCCCTGGAGGGTATCAGG-3'; gRNA4: 5'-GATCACCTCCAGGGGATTAGGG-3'; repair sequence 5'-CAGCAACTATTACAGCCTAATTTTTGTACCAGTAGGTTTATCCATGATTTTCAGTGCCTTGTTTGAAGCACCACTTAGCTAATCTCATGCCTTGCTAAATAGCTGGGCCTTTTTCTCAGCTTCTGATAGTGCTTAGTAGACACCATCTGTATTGCAAGCTCTGCCTAAGCTGTATGAATGATGCACAATTTGAAGCAGGAAAGTGAAGATGGTCTCTTAGACAGCAGGTTCTACCTCTAGGTTCTCTACGCAGAGTGTCAACAGTGGTTCTCACTTATGGGTCTCGACCCCTTTGTCGGGTAAACAATCCTTTTACAGGAGTCAGATATCCTGCATAACAGGTATTTA

CATTATGATTAATAGTAGTAGCAAAAATCACAGTTATGAAGTAGCAAGAAAAATAATTTTTATGTCTGGGGGGGCTACTACAACATGAGGAACTGTGTTAAAGCGGTTAAGCTTACGAAGGTTGAGAGACTGTGTTAAAGCTTTTATTATCTCCTCTTTCCATTGTTGGTGGCTGTGTGGCCTCTAAAGCTTGGGTGATCAGTTCCTGCTGGGGATTAGGGCCTTTAGCTGATTCACCTTAAAGGCCTTTGTGGGCAGCTTAGGGTTTTGCTGTATCAGCACGTTAACGATTAATTGAAAACAGCTCTGTCCAGAGATCCCTACTTTTCTGACTTTGTATAAGCAACCAGTGCCTGAGAAGCTGGGTTCCACCTGGATGCAAAAACAGCTCAGCACAATGGCTGAGTGGCAGCGGAATGCTGCAAAAGCCACTTGCAGCTTAGCAACTAGGAGAATGGGACTCAGTTAAGCAGTACACAGGGGGGATGGAAAGCTTCGCCCTCCTCGCACTGCTATTCTGTGAGAA TCCTCAGAGGAACAAAGCACCATCTTAAAAGTCAATTAAGAGAGCAATAGGTTTGGGGGAAGGGCTGTGAGGGAGTTTCCAGAGGAGTACCACCATGACACTGAATAATGT CACAAGCCAGTCCCTGAAGTTCAGTACGGGATGGAAA GTGACAGAAAATCCGAGTCCCTGTGGATGTGTTGGGGTT TCTTTTTGGAGACAATATAAAGAAGCGACAGATGTTCTGGATAGAAGGTGAGATAGCAGCGCTTGAAGTGTCTCCAAATGCCACTTGAGATGTGGAAGGGGGGATTTGCAACCCTCCAGTATTTGTG

Creation of Transgenic Embryos. We induced superovulation in female C57Bl6/JCrI donor mice following standard hormonal treatment with PMSG (pregnant mare's serum gonadotrophin) and HCG (human chorionic gonadotrophin) and performed pronuclear injection of fertilized mouse oocytes following the procedure described in (Vintersten et al. 2008). Superovulating females were mated with C57Bl6/JCrI male mice 46 h between the PMSG and HCG injections at the midpoint of the dark period (12/12 h, 6 AM to 6 PM light cycle). After positive plug detection in the morning, the cumulus complexes were isolated and zygotes removed with a treatment of hyaluronidase (final concentration of 0.1% [801 unit/ml]). Before injecting the CRISPR solution, we incubated the recombinant Cas9 protein (ToolGen, 31.31 pmol final) in protein buffer (20 mM Hepes pH 7.5, 150 mM KCl) with 7.8 pmol of each gRNA, 15.6 pmol of tracrRNA, and 0.16 pmol of the gblock repair construct in a total volume of 15 μ l, for 15 min at 37 °C, allowing the mix to form a functional complex. We next centrifuged the mix (1 min, 13,000 g) through a Durapore PVDF 0.22- μ m filter (Merck Millipore, USA). We injected the CRISPR–Cas9 solution into the male pronucleus of fertilized zygotes with a motor-driven manipulator-based microinjection stage. Recipient CrI:CD1(ICR) female mice were mated with sterile (vasectomized) CrI:CD1(ICR) males. Around 2 h after injections of CRISPR–Cas9 mix into fertilized zygotes, the surviving embryos were transferred into the pseudopregnant recipient female mice (around 20 embryos per recipient) following the procedure described previously (Arras et al. 2001).

Genotyping. We extracted genomic DNA from mouse tails using the QuickExtract DNA extraction kit (Epicentre) following manufacturer's instructions, and performed PCR using the Phusion Flash High-Fidelity PCR master mix (Thermo Fisher Scientific, USA). Two primer pairs were designed to bind to

the 5' and 3' flanks of the mouse sequence outside of the homology arms and to the BMR-specific sequence. PCR products were Sanger-sequenced to confirm the precise replacement of the regulatory element. Primer sequences are the following: 5' flanking_forward (mouse): 5'-TCAGTCTGTGAGCCGTTGAC-3'; 5' flanking_reverse (BMR^{repr} mouse): 5'-TAACGTGCTGATACAGCAAACC-3'; 3' flanking_forward (BMR^{repr} mouse): 5'-GCTTAGGGTTTTGCTGTATCA-3'; 3' flanking_reverse (mouse): 5'ACACAACCCAAGATCCACACG-3'.

Quantification of *Tdrd7* mRNA Levels by RT-qPCR

We quantified *Tdrd7* mRNA expression by RT-qPCR, with primers to amplify 97 bp of the mRNA spanning exons 12 and 13. We used the ribosomal *Rpl13a* gene as control. Primer sequences are the following: *Tdrd7*-fw: 5'-TGGCAATTCGATCCCGTGA-3'; *Tdrd7*-rev: 5'-GCACTTTATAGCCTGAGGGG-3'; *Rpl13a*-fw: 5'-CCCACAAGACCAAGAGAGGC-3'; *Rpl13a*-rev: 5'-CACCATCCGCTTTTCTTGTC-3'. We dissected lenses and testes/ovaries of E14.5, P1, and 12-week-old adult female and male wild-type and homozygous BMR^{repr} mice and snap-froze collected tissues in liquid nitrogen. Each tissue sample and timepoint is represented by at least three biological replicates. For adults, we pooled both lenses, testes and ovaries of a single mice to obtain one biological replicate. For P1 and E14.5 samples, we pooled all lenses, testes, and ovaries from all pups/embryos from one litter into one biological replicate. Total RNA was extracted with a standard TRIzol RNA extraction and chloroform/isopropanol precipitation and cDNA was prepared with the ProtoScript II First Strand cDNA synthesis kit (New England Biolabs, Frankfurt, Germany). For each sample, we collected at least three biological replicates, and measured each at least three times (technical replicates) in the LightCycler96 (Roche, Germany). We detected expression using SYBRgreen marker (Roche, Germany). To obtain the normalized expression values of *Tdrd7* in BMR^{repr} samples with respect to the wild-type condition, we followed the procedure described in (Taylor et al. 2019). In short, we computed the ΔCq of each BMR^{repr} sample with respect to the average of wild-type samples, corrected those for primer efficiency, and normalized by the control gene *Rpl13a*. We tested the difference in normalized *Tdrd7* expression between wild-type and BMR^{repr} mice with a two-sided *t*-test.

Absolute Quantification of TDRD7 Protein by MS Western

We opted for an absolute quantification of TDRD7 protein in developing lenses using MS-Western (Kumar et al. 2018). TDRD7 was quantified by codigestion of its SDS-PAGE-separated band with the band of isotopically labeled chimera composed of concatenated proteotypic peptides.

Preparation of Labeled TDRD7 Peptides

We selected quantotypic peptides for TDRD7 protein using the collection of mass spectra available in the MaxQB database (supplementary table 3, Supplementary Material online),

according to (Rauniyar 2015). Peptide sequences were included into an *Escherichia coli*-optimized synthetic gene construct containing a TwinStrep tag, selected phosB and BSA peptides (Kumar et al. 2018). The construct was cloned into a pET expression vector and transformed into a BL21 (DE3) *E. coli* strain, auxotrophic for arginine and lysine. Cells were grown at 37 °C in MDAG-135 media (Studier 2005), supplemented with 16 unlabeled amino acids and isotopically labeled ¹³C₆¹⁵N₄-l-arginine and ¹³C₆-l-lysine (Silantes, Munich, Germany). Protein expression was induced by 1-mM isopropyl β -D-1-thiogalactopyranoside (IPTG) for 3 h. After induction, cells were pelleted, resuspended in 2× PBS, snap-frozen in liquid nitrogen, and stored at −80 °C. Prior to analyses, cells were thawed and lysed in an equal volume of 2× Laemmli buffer by incubating at 95 °C for 10 min. The sample was clarified by centrifugation and the supernatant subjected to 1D SDS-PAGE on a 4–20% precast gradient gel. Proteins were visualized by Coomassie staining.

Sample Preparation

We carefully dissected the lenses of wild-type and homozygous BMR^{repr} E14.5 embryos and P1 pups (2 biological replicates for E14.5 samples and a single replicate for P1), snap-froze them in liquid nitrogen and stored at −80 °C until use. To lyse the tissue, we added 40 μ l of 1× Laemmli buffer with 0.5 μ l of protease inhibitors cocktail (Thermo Fischer Scientific, USA) and 20–30 0.2-mm stainless steel beads (Next Advance, USA) per vial, and homogenized it in a TissueLyser (Qiagen, Düsseldorf, Germany) for 10 min at 4 °C. Homogenized material was centrifuged for 10 min and heated at 80 °C for 5 min. After cooling down to room temperature, cell debris was spun down and the supernatant loaded onto a 1D SDS min-gel (BioRad Laboratories, USA). We visualized the gel by Coomassie staining and excised the region corresponding to the molecular weight of TDRD7 protein for subsequent MS-Western analysis.

Mass Spectrometric Analysis and Absolute Quantification Using MS-Western

Absolute quantification of TDRD7 protein was performed as described in (Kumar et al. 2018). Briefly, an aliquot of 0.5 pmol of BSA standard (Thermo Fischer Scientific, USA) was analyzed by 1D SDS-PAGE, visualized by Coomassie, and the BSA band was excised. The gel slices containing TDRD7, the isotopically labelled chimeric protein standard from a separate gel, and a band of the BSA standard were combined together. Proteins were reduced with 10 mM DTT, alkylated by iodiacetamide and in-gel digested overnight with trypsin. The resulting peptide mixture was extracted twice by exchange of 5% formic acid and acetonitrile, extracts pooled together and dried in a vacuum centrifuge. Peptides were resuspended in 25 μ l of 5% FA and a 5 μ l aliquot was analyzed by LC-MS/MS on a nano-UPLC system interfaced to a Q Exactive HF Orbitrap mass spectrometer (both Thermo Fischer Scientific, Bremen, Germany). The nano-UPLC was equipped with an Acclaim PepMap100 C18 75 μ m i.d. × 20-mm trap column and 75 μ m × 15-cm analytical column

(3 $\mu\text{m}/100\text{A}$, Thermo Fisher Scientific, Bremen, Germany). Peptides were separated using an 80-min linear gradient: solvent A was 0.1% aqueous formic acid and solvent B was 0.1% formic acid in neat acetonitrile. Three blank runs were performed after each sample analysis to minimize carryover, the last blank run was recorded and searched against mouse sequences in UniProt database. To set up PRM parameters, the relevant information on target peptides (m/z , charge state, retention time; [supplementary fig. 1, Supplementary Material](#) online) was obtained in preliminary experiments using a tryptic digest of the chimeric standard. In all experiments, FT MS spectrum was acquired within the mass range of m/z 350–1,700 at the mass resolution of $R_{m/z=200} = 240,000$ (FWHM); target AGC of 3×10^6 , 150-ms maximum injection time. It was followed by PRM scans at $R_{m/z=200} = 120,000$ resolution; target AGC of 1×10^5 ; 200-ms maximum injection time triggered by a scheduled inclusion list. Lock mass was set to the singly charged ion of dodecamethylcyclohexasiloxane ion ($(\text{Si}(\text{CH}_3)_2\text{O})_6$; $m/z = 445.1200$).

We processed the spectra using the SkyLine software ([MacLean et al. 2010](#)). We manually verified the data, refining the peak boundaries where necessarily. MS/MS spectra from PRM experiments were also searched with MASCOT software against a database of mouse protein sequences. Quantification was performed using the sum of extracted peak areas of 2–4 most abundant y -ion fragments whose m/z exceeded the m/z of the corresponding precursor ion and integral value exceeding 1×10^6 . First, the amount of each labelled standard peptide was quantified using the peak areas of peptides of unlabelled BSA standard (note that all peptides in chimera standard protein, including peptides from BSA and TDRD7, were present in equimolar ratios). Then, the molar abundance of the labelled standard peptides was used to quantify peptides from endogenous TDRD7. As data quality control, we required that normalized ratios of fragment ion abundances were the same in labelled (from chimera) and corresponding unlabelled (endogenous) peptides. Finally, the data were normalized to the number of eye lenses pooled in each sample.

Analyzing Lens Morphology

Quantifying Nuclear Cataracts

To quantify the number and size of cataract aggregates in the lenses of adult mice, we imaged them with an Olympus SZX16 stereoscope equipped with a q-Imaging camera. We carefully dissected the lenses of wild-type and homozygous BMR^{repr} mice with ages between 6 months and 1.5 years, immediately embedded them in Optiprep refractive index matching media ([Boothe et al. 2017](#)), and imaged under dark-field illumination (11.5 \times magnification; 250 ms exposure and 6.5 gain). We used Fiji ([Schindelin et al. 2012](#)) to process images with a script that includes subtracting background (rolling ball radius = 50 pixels), median filtering (radius = 2 pixels), detecting objects with the Interactive Watershed plugin (SCF; seed dynamics 2,000, intensity threshold 4,000, peak flooding 50, AllowSplitting = false), and finally obtaining the number and size of elements with Analyze Particles plugin (size = 1,000–10,000 px^2).

We performed a post hoc power analysis using the R package `pwr` (function `pwr.t.test`) to estimate the sample size one would need to get 80% power to detect a significant effect at $P < 0.05$ for a two-sided t -test. Effect size was determined as the difference in the mean number of cataract aggregates between the 0.5- and 1-year-old wild-type and BMR^{repr} mice (4.4736 and 6.0625, respectively), divided by the observed standard deviation (3.17). This resulted in an estimated sample size of 63.46. Pooling the data for young and 1.5-year-old BMR^{repr} mice estimated a sample size of 187.15.

Scanning Electron Microscopy

Lenses of 2-year-old wild-type and homozygous BMR^{repr} mice aged were carefully dissected and fixed in a modified Karnovsky's fixative (2% glutaraldehyde/2% formaldehyde in 100-mM phosphate buffer) at 4 $^\circ\text{C}$ for at least one day to allow the fixative to penetrate through the more external layers of the lens. After this period, the lenses were cut in half through the equatorial plane and fixed again in the same solution for at least another 3 days. Samples were washed with PBS (10 mM Na_2HPO_4 , 1.8 mM KH_2PO_4 , 137 mM NaCl, 2.7 mM KCl, pH 7.4) for 5×5 min. After that, the material was postfixed in 1% osmium tetroxide in PBS, washed several times in PBS and water, and dehydrated in a graded series of ethanol/water mixtures up to pure ethanol (30%, 50%, 70%, 96%, and $3 \times 100\%$ on molecular sieve, 15 min each). Samples were critical point dried using a Leica CPD300 (Leica Microsystems, Wetzlar, Germany) and mounted on 12-mm aluminum stubs using conductive carbon tabs. The lens halves were additionally grounded with conductive liquid silver paint. To increase contrast and conductivity, the samples were sputter coated with gold (BAL-TEC SCD 050 sputter coater, settings: 60 s, with 60 mA, at 5-cm working distance). Finally, the samples were imaged with a JSM 7500 F scanning electron microscope (JEOL, Garching, Germany) running at 5 kV (lower SE-detector, working distance 8 mm).

Analyzing Sperm Quality

To characterize potential differences in sperm quality between wild-type and homozygous BMR^{repr} adult mice, we collected sperm samples and analyzed them on an automated sperm analyzer. Sample preparation followed ([Helppi et al. 2016](#)). In short, we dissected the epididymis of age-matched wild-type and BMR^{repr} mice (three biological replicates), embedded it in 170 μl of cryoprotective agent (18% raffinose and 3% skim milk), and transferred equal amounts of the sperm solution to human tubal fluid, to a concentration of 1:50. We then added this solution to a Standard Count 2 Chamber Slide from Leja (Nieuw-Vennep, The Netherlands) and measurements were made with a Hamilton Thorne Automated Sperm Analyser (Hamilton Thorne, Beverly, MA, USA) with default settings for mouse sperm.

Supplementary Material

Supplementary data are available at *Molecular Biology and Evolution* online.

Acknowledgments

We thank Maurício de Rocha Martins for helpful discussions and comments on the manuscript, Salil Lachke for providing the lens cell line, Andrea Schuhmann for assistance in MS experiments and analyses, and the following MPI-CBG facilities for their support: Antibody Facility, Biomedical services, Cell Technologies Group, DNA sequencing, Mass Spectrometry, Transgenic Core Facility, TransgeneOmics, and Technology Development Studio. This work was supported by the Max Planck Society.

References

- Abd El-Aziz MM, Barragan I, O'Driscoll CA, Goodstadt L, Prigmore E, Borrego S, Mena M, Pieras JJ, El-Ashry MF, Safieh LA, et al. 2008. EYS, encoding an ortholog of *Drosophila* spacemaker, is mutated in autosomal recessive retinitis pigmentosa. *Nat Genet.* 40(11):1285–1287.
- Ahituv N, Zhu Y, Visel A, Holt A, Afzal V, Pennacchio LA, Rubin EM. 2007. Deletion of ultraconserved elements yields viable mice. *PLoS Biol.* 5(9):e234.
- Arras M, Autenried P, Rettich A, Spaeni D, Rulicke T. 2001. Optimization of intraperitoneal injection anesthesia in mice: drugs, dosages, adverse effects, and anesthesia depth. *Comp Med.* 51(5):443–456.
- Bailey TL, Gribskov M. 1998. Combining evidence using *P*-values: application to sequence homology searches. *Bioinformatics* 14(1):48–54.
- Boothe T, Hilbert L, Heide M, Berninger L, Huttner WB, Ziburdaev V, Vastenhouw NL, Myers EW, Drechsel DN, Rink JC. 2017. A tunable refractive index matching medium for live imaging cells, tissues and model organisms. *eLife* 6:e27240.
- Capellini TD, Chen H, Cao J, Doxey AC, Kiapour AM, Schoor M, Kingsley DM. 2017. Ancient selection for derived alleles at a GDF5 enhancer influencing human growth and osteoarthritis risk. *Nat Genet.* 49(8):1202–1210.
- Carroll SB. 2008. Evo-devo and an expanding evolutionary synthesis: a genetic theory of morphological evolution. *Cell* 134(1):25–36.
- Castro JP, Yancoskie MN, Marchini M, Belohlavy S, Hiramatsu L, Kucka M, Beluch WH, Naumann R, Skuplik I, Cobb J, et al. 2019. An integrative genomic analysis of the Longshanks selection experiment for longer limbs in mice. *eLife* 8:e42014.
- Catania KC. 1999. A nose that looks like a hand and acts like an eye: the unusual mechanosensory system of the star-nosed mole. *J Comp Physiol A* 185(4):367–372.
- Chan YF, Marks ME, Jones FC, Villarreal G Jr, Shapiro MD, Brady SD, Southwick AM, Absher DM, Grimwood J, Schmutz J, et al. 2010. Adaptive evolution of pelvic reduction in sticklebacks by recurrent deletion of a *Pitx1* enhancer. *Science* 327(5963):302–305.
- Cooper HM, Herbin M, Nevo E. 1993a. Ocular regression conceals adaptive progression of the visual system in a blind subterranean mammal. *Nature* 361(6408):156–159.
- Cooper HM, Herbin M, Nevo E. 1993b. Visual system of a naturally microphthalmic mammal: the blind mole rat, *Spalax ehrenbergi*. *J Comp Neurol.* 328(3):313–350.
- Corbo JC, Lawrence KA, Karlstetter M, Myers CA, Abdelaziz M, Dirkes W, Weigelt K, Seifert M, Benes V, Fritsche LG, et al. 2010. CRX ChIP-seq reveals the *cis*-regulatory architecture of mouse photoreceptors. *Genome Res.* 20(11):1512–1525.
- Cretokos CJ, Wang Y, Green ED, Martin JF, Rasweiler JTT, Behringer RR. 2008. Regulatory divergence modifies limb length between mammals. *Genes Dev.* 22(2):141–151.
- Davydov EV, Goode DL, Sirota M, Cooper GM, Sidow A, Batzoglou S. 2010. Identifying a high fraction of the human genome to be under selective constraint using GERP. *PLoS Comput Biol.* 6(12):e1001025.
- Emerling CA, Springer MS. 2014. Eyes underground: regression of visual protein networks in subterranean mammals. *Mol Phylogenet Evol.* 78:260–270.
- Emerling CA, Widjaja AD, Nguyen NN, Springer MS. 2017. Their loss is our gain: regressive evolution in vertebrates provides genomic models for uncovering human disease loci. *J Med Genet.* 54(12):787–794.
- Encode Project Consortium. 2012. An integrated encyclopedia of DNA elements in the human genome. *Nature* 489:57–74.
- Fang X, Nevo E, Han L, Levanon EY, Zhao J, Avivi A, Larkin D, Jiang X, Feranchuk S, Zhu Y, et al. 2014. Genome-wide adaptive complexes to underground stresses in blind mole rats *Spalax*. *Nat Commun.* 5(1):3966.
- Fang X, Seim I, Huang Z, Gerashchenko MV, Xiong Z, Turanov AA, Zhu Y, Lobanov AV, Fan D, Yim SH, et al. 2014. Adaptations to a subterranean environment and longevity revealed by the analysis of mole rat genomes. *Cell Rep.* 8(5):1354–1364.
- Frankel N, Davis GK, Vargas D, Wang S, Payre F, Stern DL. 2010. Phenotypic robustness conferred by apparently redundant transcriptional enhancers. *Nature* 466(7305):490–493.
- Fuchsberger C, Flannick J, Teslovich TM, Mahajan A, Agarwala V, Gaulton KJ, Ma C, Fontanillas P, Moutsianas L, McCarthy DJ, et al. 2016. The genetic architecture of type 2 diabetes. *Nature* 536(7614):41–47.
- Fulco CP, Nasser J, Jones TR, Munson G, Bergman DT, Subramanian V, Grossman SR, Anyoha R, Doughty BR, Patwardhan TA, et al. 2019. Activity-by-contact model of enhancer–promoter regulation from thousands of CRISPR perturbations. *Nat Genet.* 51(12):1664–1669.
- Gaudry MJ, Jastroch M, Treberg JR, Hofreiter M, Pajjmans JLA, Starrett J, Wales N, Signore AV, Springer MS, Campbell KL. 2017. Inactivation of thermogenic UCP1 as a historical contingency in multiple placental mammal clades. *Sci Adv.* 3(7):e1602878.
- Gonen N, Futtner CR, Wood S, Garcia-Moreno SA, Salamone IM, Samson SC, Sekido R, Poulat F, Maatouk DM, Lovell-Badge R. 2018. Sex reversal following deletion of a single distal enhancer of *Sox9*. *Science* 360(6396):1469–1473.
- Grunwald HA, Gantz VM, Poplawski G, Xu XS, Bier E, Cooper KL. 2019. Super-Mendelian inheritance mediated by CRISPR–Cas9 in the female mouse germline. *Nature* 566(7742):105–109.
- Guo M, Liu X, Willen J, Shaw CP, Richard D, Jagoda E, Doxey AC, Hirschhorn J, Capellini TD. 2017. Epigenetic profiling of growth plate chondrocytes sheds insight into regulatory genetic variation influencing height. *eLife* 6:e29329.
- Hansen L, Yao W, Eiberg H, Kjaer KW, Baggesen K, Hejtmancik JF, Rosenberg T. 2007. Genetic heterogeneity in microcornea–cataract: five novel mutations in CRYAA, CRYGD, and GJA8. *Invest Ophthalmol Vis Sci.* 48(9):3937–3944.
- Hao H, Kim DS, Klocke B, Johnson KR, Cui K, Gotoh N, Zang C, Gregorski J, Gieser L, Peng W, et al. 2012. Transcriptional regulation of rod photoreceptor homeostasis revealed by in vivo NRL targetome analysis. *PLoS Genet.* 8(4):e1002649.
- Hecker N, Sharma V, Hiller M. 2019. Convergent gene losses illuminate metabolic and physiological changes in herbivores and carnivores. *Proc Natl Acad Sci U S A.* 116(8):3036–3041.
- Helppi J, Schreier D, Naumann R, Zierau O. 2016. Mouse reproductive fitness is maintained up to an ambient temperature of 28 when housed in individually-ventilated cages. *Lab Anim.* 50(4):254–263.
- Hetling JR, Baig-Silva MS, Comer CM, Pardue MT, Samaan DY, Qtaishat NM, Pepperberg DR, Park TJ. 2005. Features of visual function in the naked mole-rat *Heterocephalus glaber*. *J Comp Physiol A* 191(4):317–330.
- Hosokawa M, Shoji M, Kitamura K, Tanaka T, Noce T, Chuma S, Nakatsuiji N. 2007. Tudor-related proteins TDRD1/MTR-1, TDRD6 and TDRD7/TRAP: domain composition, intracellular localization, and function in male germ cells in mice. *Dev Biol.* 301(1):38–52.
- Huelsmann M, Hecker N, Springer MS, Gatesy J, Sharma V, Hiller M. 2019. Genes lost during the transition from land to water in cetaceans highlight genomic changes associated with aquatic adaptations. *Sci Adv.* 5(9):eaaw6671.
- International Schizophrenia Consortium, Purcell SM, Wray NR, Stone JL, Visscher PM, O'Donovan MC, Sullivan PF, Sklar P. 2009. Common

- polygenic variation contributes to risk of schizophrenia and bipolar disorder. *Nature* 460(7256):748–752.
- Kim EB, Fang X, Fushan AA, Huang Z, Lobanov AV, Han L, Marino SM, Sun X, Turanov AA, Yang P, et al. 2011. Genome sequencing reveals insights into physiology and longevity of the naked mole rat. *Nature* 479(7372):223–227.
- Kumar M, Joseph SR, Augsburg M, Bogdanova A, Drechsel D, Vastenhouw NL, Buchholz F, Gentzel M, Shevchenko A. 2018. MS Western, a method of multiplexed absolute protein quantification is a practical alternative to Western blotting. *Mol Cell Proteomics* 17(2):384–396.
- Kvon EZ, Kamneva OK, Melo US, Barozzi I, Osterwalder M, Mannion BJ, Tissières V, Pickle CS, Plajzer-Frick I, Lee EA, et al. 2016. Progressive loss of function in a limb enhancer during snake evolution. *Cell* 167(3):633–642.e611.
- Lachke SA, Alkuraya FS, Kneeland SC, Ohn T, Aboukhalil A, Howell GR, Saadi I, Cavallese R, Yue Y, Tsai AC, et al. 2011. Mutations in the RNA granule component TDRD7 cause cataract and glaucoma. *Science* 331(6024):1571–1576.
- Langer BE, Hiller M. 2019. TFforge utilizes large-scale binding site divergence to identify transcriptional regulators involved in phenotypic differences. *Nucleic Acids Res.* 47(4):e19.
- Langer BE, Roscito JG, Hiller M. 2018. REforge associates transcription factor binding site divergence in regulatory elements with phenotypic differences between species. *Mol Biol Evol.* 35(12):3027–3040.
- MacLean B, Tomazela DM, Shulman N, Chambers M, Finney GL, Frewen B, Kern R, Tabb DL, Liebler DC, MacCoss MJ. 2010. Skyline: an open source document editor for creating and analyzing targeted proteomics experiments. *Bioinformatics* 26(7):966–968.
- Makiyama Y, Ooto S, Hangai M, Ogino K, Gotoh N, Oishi A, Yoshimura N. 2014. Cone abnormalities in fundus albipunctatus associated with RDH5 mutations assessed using adaptive optics scanning laser ophthalmoscopy. *Am J Ophthalmol.* 157(3):558–570.e551–554.
- Mattapallil MJ, Wawrousek EF, Chan CC, Zhao H, Roychoudhury J, Ferguson TA, Caspi RR. 2012. The Rd8 mutation of the Crb1 gene is present in vendor lines of C57BL/6N mice and embryonic stem cells, and confounds ocular induced mutant phenotypes. *Invest Ophthalmol Vis Sci.* 53(6):2921–2927.
- Meredith RW, Gates J, Murphy WJ, Ryder OA, Springer MS. 2009. Molecular decay of the tooth gene Enamelin (ENAM) mirrors the loss of enamel in the fossil record of placental mammals. *PLoS Genet.* 5(9):e1000634.
- Meyer WK, Jamison J, Richter R, Woods SE, Partha R, Kowalczyk A, Kronk C, Chikina M, Bonde RK, Crocker DE, et al. 2018. Ancient convergent losses of Paraoxonase 1 yield potential risks for modern marine mammals. *Science* 361(6402):591–594.
- Mo A, Luo C, Davis FP, Mukamel EA, Henry GL, Nery JR, Urlich MA, Picard S, Lister R, Eddy SR, et al. 2016. Epigenomic landscapes of retinal rods and cones. *eLife* 5:e11613.
- Moore BA, Leonard BC, Sebbag L, Edwards SG, Cooper A, Imai DM, Straiton E, Santos L, Reilly C, Griffey SM, et al. 2018. Identification of genes required for eye development by high-throughput screening of mouse knockouts. *Commun Biol.* 1(1):236.
- Němec P, Cveková P, Benada O, Wielkopolaska E, Olkowicz S, Turlejski K, Burda H, Bennett NC, Peichl L. 2008. The visual system in subterranean African mole-rats (Rodentia, Bathyergidae): retina, subcortical visual nuclei and primary visual cortex. *Brain Res Bull.* 75(2–4):356–364.
- Nevo E. 2007. Mosaic evolution of subterranean mammals: tinkering, regression, progression, and global convergence. In: Begall S, Burda H, Schleich CE, editors. Subterranean rodents: news from the underground. Berlin, Heidelberg: Springer. p. 375–388.
- Osterwalder M, Barozzi I, Tissières V, Fukuda-Yuzawa Y, Mannion BJ, Afzal SY, Lee EA, Zhu Y, Plajzer-Frick I, Pickle CS, et al. 2018. Enhancer redundancy provides phenotypic robustness in mammalian development. *Nature* 554(7691):239–243.
- Partha R, Chauhan BK, Ferreira Z, Robinson JD, Lathrop K, Nischal KK, Chikina M, Clark NL. 2017. Subterranean mammals show convergent regression in ocular genes and enhancers, along with adaptation to tunneling. *eLife* 6:e25884.
- Prudent X, Parra G, Schwede P, Roscito JG, Hiller M. 2016. Controlling for phylogenetic relatedness and evolutionary rates improves the discovery of associations between species' phenotypic and genomic differences. *Mol Biol Evol.* 33(8):2135–2150.
- Quinlan AR, Hall IM. 2010. BEDTools: a flexible suite of utilities for comparing genomic features. *Bioinformatics* 26(6):841–842.
- Rauniyar N. 2015. Parallel reaction monitoring: a targeted experiment performed using high resolution and high mass accuracy mass spectrometry. *IJMS* 16(12):28566–28581.
- Remington L. 2012. Chapter 5 - crystalline lens. In: Remington L, Goodwin D, editors. Clinical anatomy and physiology of the visual system. St. Louis: Elsevier. p. 93–108.
- Roscito JG, Sameith K, Parra G, Langer BE, Petzold A, Moebius C, Bickle M, Rodrigues MT, Hiller M. 2018. Phenotype loss is associated with widespread divergence of the gene regulatory landscape in evolution. *Nat Commun.* 9(1):4737.
- Samuel A, Housset M, Fant B, Lamonerie T. 2014. Otx2 ChIP-seq reveals unique and redundant functions in the mature mouse retina. *PLoS One* 9(2):e89110.
- Sanyal S, Jansen HG, de Grip WJ, Nevo E, de Jong WW. 1990. The eye of the blind mole rat, *Spalax ehrenbergi*. Rudiment with hidden function? *Invest Ophthalmol Vis Sci.* 31(7):1398–1404.
- Sarro R, Kocher AA, Emera D, Uebbing S, Dutrow EV, Weatherbee SD, Nottoli T, Noonan JP. 2018. Disrupting the three-dimensional regulatory topology of the Pitx1 locus results in overtly normal development. *Development* 145(7):dev158550.
- Schindelin J, Arganda-Carreras I, Frise E, Kaynig V, Longair M, Pietzsch T, Preibisch S, Rueden C, Saalfeld S, Schmid B, et al. 2012. Fiji: an open-source platform for biological-image analysis. *Nat Methods* 9(7):676–682.
- Sharma V, Hecker N, Roscito JG, Foerster L, Langer BE, Hiller M. 2018. A genomics approach reveals insights into the importance of gene losses for mammalian adaptations. *Nat Commun.* 9(1):1215.
- Sharma V, Hiller M. 2018. Loss of enzymes in the bile acid synthesis pathway explains differences in bile composition among mammals. *Genome Biol Evol.* 10(12):3211–3217.
- Sharma V, Hiller M. 2020. Losses of human disease-associated genes in placental mammals. *NAR Genomics Bioinform.* 2(1):lqz012.
- Sharma V, Lehmann T, Stuckas H, Funke L, Hiller M. 2018. Loss of RXFP2 and INSL3 genes in Afrotheria shows that testicular descent is the ancestral condition in placental mammals. *PLoS Biol.* 16(6):e2005293.
- Siepel A, Bejerano G, Pedersen JS, Hinrichs AS, Hou M, Rosenbloom K, Clawson H, Spieth J, Hillier LW, Richards S, et al. 2005. Evolutionarily conserved elements in vertebrate, insect, worm, and yeast genomes. *Genome Res.* 15(8):1034–1050.
- Stingele S, Stoehr G, Peplowska K, Cox J, Mann M, Storchova Z. 2012. Global analysis of genome, transcriptome and proteome reveals the response to aneuploidy in human cells. *Mol Syst Biol.* 8:608.
- Studier FW. 2005. Protein production by auto-induction in high density shaking cultures. *Protein Expr Purif.* 41(1):207–234.
- Sweet G. 1909. The eyes of *Chrysochloris hottentota* and *C. asiatica*. *J Cell Sci.* s2–52:327–338.
- Tan YQ, Tu C, Meng L, Yuan S, Sjaarda C, Luo A, Du J, Li W, Gong F, Zhong C, et al. 2019. Loss-of-function mutations in TDRD7 lead to a rare novel syndrome combining congenital cataract and nonobstructive azoospermia in humans. *Genet Med.* 21(5):1209–1217.
- Tanaka T, Hosokawa M, Vagin VV, Reuter M, Hayashi E, Mochizuki AL, Kitamura K, Yamanaka H, Kondoh G, Okawa K, et al. 2011. Tudor domain containing 7 (Tdrd7) is essential for dynamic ribonucleoprotein (RNP) remodeling of chromatoid bodies during spermatogenesis. *Proc Natl Acad Sci U S A.* 108(26):10579–10584.
- Taylor SC, Nadeau K, Abbasi M, Lachance C, Nguyen M, Fenrich J. 2019. The ultimate qPCR experiment: producing publication quality, reproducible data the first time. *Trends Biotechnol.* 37(7):761–774.
- Thompson AC, Capellini TD, Guenther CA, Chan YF, Infante CR, Menke DB, Kingsley DM. 2018. A novel enhancer near the Pitx1 gene

- influences development and evolution of pelvic appendages in vertebrates. *eLife* 7:e38555.
- Vintersten K, Testa G, Naumann R, Anastasiadis K, Stewart AF. 2008. Bacterial artificial chromosome transgenesis through pronuclear injection of fertilized mouse oocytes. *Methods Mol Biol.* 415:83–100.
- Wray GA. 2007. The evolutionary significance of *cis*-regulatory mutations. *Nat Rev Genet.* 8(3):206–216.
- Yang J, Benyamin B, McEvoy BP, Gordon S, Henders AK, Nyholt DR, Madden PA, Heath AC, Martin NG, Montgomery GW, et al. 2010. Common SNPs explain a large proportion of the heritability for human height. *Nat Genet.* 42(7):565–569.
- Zhang F, Lupski JR. 2015. Non-coding genetic variants in human disease. *Hum Mol Genet.* 24(R1):R102–110.
- Zhao Y, Zheng D, Cvekl A. 2019. Profiling of chromatin accessibility and identification of general *cis*-regulatory mechanisms that control two ocular lens differentiation pathways. *Epigenet Chromatin* 12(1):27.